

# Rainfall, ground-water flow, and seasonal movement at Minor Creek landslide, northwestern California: Physical interpretation of empirical relations

RICHARD M. IVERSON } U.S. Geological Survey, Cascades Volcano Observatory, 5400 MacArthur Blvd., Vancouver, Washington 98661  
JON J. MAJOR }

## ABSTRACT

Simple ground-water flow analyses can clarify complex empirical relations between rainfall and landslide motion. Here we present detailed data on rainfall, ground-water flow, and repetitive seasonal motion that occurred from 1982 to 1985 at Minor Creek landslide in northwestern California, and we interpret these data in the context of physically based theories. We find that landslide motion is closely regulated by the direction and magnitude of near-surface hydraulic gradients and by waves of pore pressure caused by intermittent rainfall.

Diffusive propagation of pore-pressure waves accompanies downward ground-water flow along nearly vertical hydraulic gradients that exist in most of the landslide. Field data combined with a pore-pressure diffusion analysis show that single rainstorms typically produce short-period waves that attenuate before reaching the landslide base. In contrast, seasonal rainfall cycles produce long-period waves that modify basal pore pressures, but only after time lags that range from weeks to months. Such time lags can depend on antecedent moisture storage and can explain variable delays between the onset of the wet season and seasonal landslide motion.

Limit-equilibrium analysis shows that when seasonal pressure waves reach the landslide base, they establish a critical distribution of effective stress that delicately triggers landslide motion. The critical effective-stress balance is extremely sensitive to the direction and magnitude of hydraulic gradients.

Although pervasively downward gradients instigate seasonal motion, we infer from theory and limited data that ground water also may circulate locally in near-surface cells. The circulation can further reduce the landslide's frictional strength, particularly in areas of nearly horizontal ground-water flow that occur beneath steep faces of hummocks. Hummocky topography that results from slope instability may therefore cause ground-water flow that perpetuates instability.

## INTRODUCTION

Ground water strongly influences the effective stress state in earth materials and can therefore precipitate hillslope instability (Terzaghi, 1923, 1943, 1950). A variety of theoretical studies have clarified the destabilizing role of steady, Darcian ground-water flow in slopes (Patton and Hendron, 1974; Hodge and Freeze, 1977; Iverson and Major, 1986). Only recently, however, have quantitative studies addressed the destabilizing role of transiently recharging ground-water flow (Leach and Herbert, 1982; Humphreys, 1982; Kenney and Lau, 1984; Sangrey and others, 1984; Wilson and others, 1984; Reid and others, 1985), and these studies typically have focused on short-term water-table fluctuations that can cause abrupt failures in static slopes. Few, if any, studies have focused on spatially variable, transient ground-water flow that repeatedly affects the motion of persistent landslides.

In this paper, we present results of a detailed, 3-yr, hydrogeologic and geomorphologic investigation of the persistently active Minor Creek landslide in northwestern California. The landslide moves significant distances each rainy sea-

son; however, the timing, duration, and speed of movement do not correlate directly with the timing and amount of rainfall. Other investigators also have found complex relationships between rainfall and intermittent movements of active landslides (Prior and Stephens, 1972; Kelsey, 1978; Vandine, 1980; Wasson and Hall, 1982; Keefer and Johnson, 1983; Swanson and others, 1983; Bertini and others, 1984; Nadler, 1984), motivating much conjecture about the causal link between rainfall and movement, and thwarting most attempts to use rainfall as a statistical predictor of motion (Ziemer, 1984).

To understand the influence of rainfall recharge and spatially variable ground-water flow on landslide motion, we have collected detailed rainfall, ground-water, and movement data at Minor Creek landslide and analyzed them in the context of simple, physically based theories. On the basis of our analyses, we infer that persistent downward hydraulic gradients, unsaturated ground-water storage, propagation and attenuation of rainfall-induced pore-pressure waves, and near-surface ground-water circulation can influence landslide motion profoundly.

## FIELD SETTING AND DATA COLLECTION

Minor Creek landslide, a compound, complex, earthflow-like landslide (compare Varnes, 1978), covers about 10 hectares (ha) in the Redwood Creek drainage basin of northwestern California (Fig. 1). Aerial photographs indicate that the landslide is at least 50 yr old, but it probably is much older. The surface of the landslide is hummocky and stepped (Fig. 2). On average, however, it slopes uniformly to the south at an angle of 15° (Fig. 3). The landslide

Additional material (Appendix) for this article may be secured free of charge by requesting Supplementary Data 87-24 from the GSA Documents Secretary.

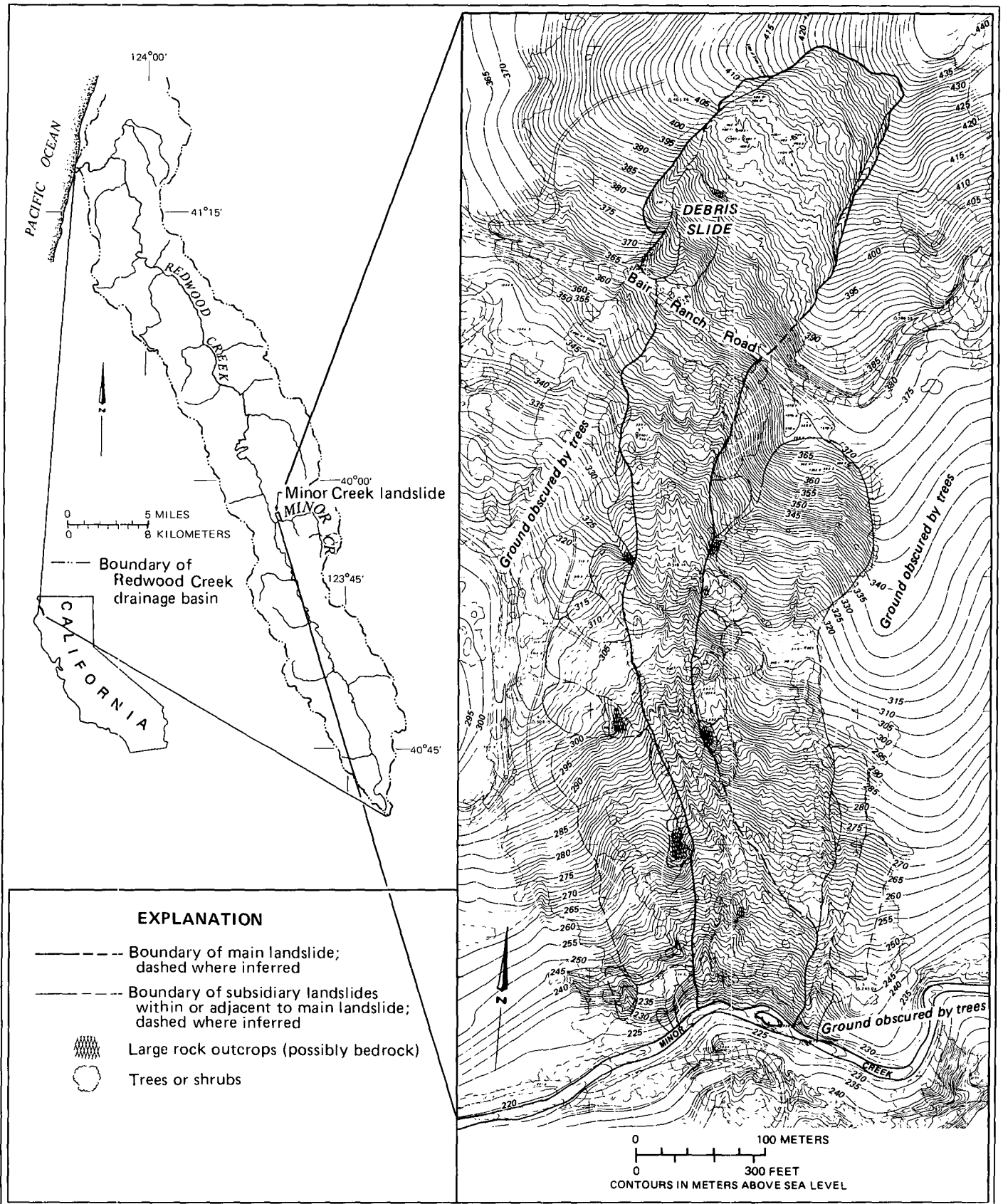


Figure 1. Location and topography of Minor Creek landslide, mapped photogrammetrically in 1982.

heads near a topographic divide, and its toe adjoins the channel of Minor Creek, a perennial tributary of Redwood Creek. Inclinator data indicate that shear deformation along the landslide base occurs in a zone about 1 m thick. Above this zone, the landslide moves chiefly as a rigid body that, where measured, ranges from about 4 m thick near its lateral margins to 6 m thick near its longitudinal axis (Iverson, 1984, 1985a). In many respects, the morphology of Minor Creek landslide resembles that of other slow-moving landslides in the area, such as the Halloween earthflow (Kelsey, 1978).

The relations of climate, bedrock geology, and land use to hillslope mass movement in the Redwood Creek basin have been described elsewhere (Colman, 1973; Harden and others, 1978; Janda, 1979; Swanston and others, 1983). Briefly, the basin consists largely of accreted Franciscan terrane composed of fractured and metamorphosed rocks (Harden and others, 1982). High seasonal rainfall, steep topography, and deep weathering make slopes underlain by these rocks very susceptible to several styles of mass movement (Nolan and others, 1976).

Rock outcrops are widely scattered at Minor Creek landslide (Fig. 1), and landslide deformation occurs in weathered, clay-rich regolith material, which envelopes many granule- to boulder-sized rock fragments. We refer to the regolith, including rock fragments that are gravel-sized and smaller, as "soil." Borings indicate that the soil extends locally to depths at least as great as 17 m, and shallow seismic refraction profiles indicate that its depth might be considerably greater (Bromirski and Dengler, 1985). Rock fragments in the soil consist primarily of slightly metamorphosed litharenitic sandstone and mudstone, with some greenstone and chert.

The Redwood Creek basin has a Mediterranean climate, and the mean annual precipitation in the vicinity of Minor Creek landslide is about 2 m. Nearly all precipitation occurs as rainfall, more than 80% of which typically falls between October and April. Because days usually are cloudy and cool during the rainy season, evaporation is slight, and most rain infiltrates the soil. Considerable surface-water ponding in abundant, shallow, closed depressions on the landslide nevertheless occurs during winter and spring. Ponding is particularly prevalent near seeps below steep faces of hummocks. During summer, seeps and ponds disappear, and the ground surface becomes hard and dry. Little overland flow occurs on Minor Creek landslide except within gullies and where livestock have compacted the soil. The landslide is vegetated primarily by grasses and forbs, with scattered

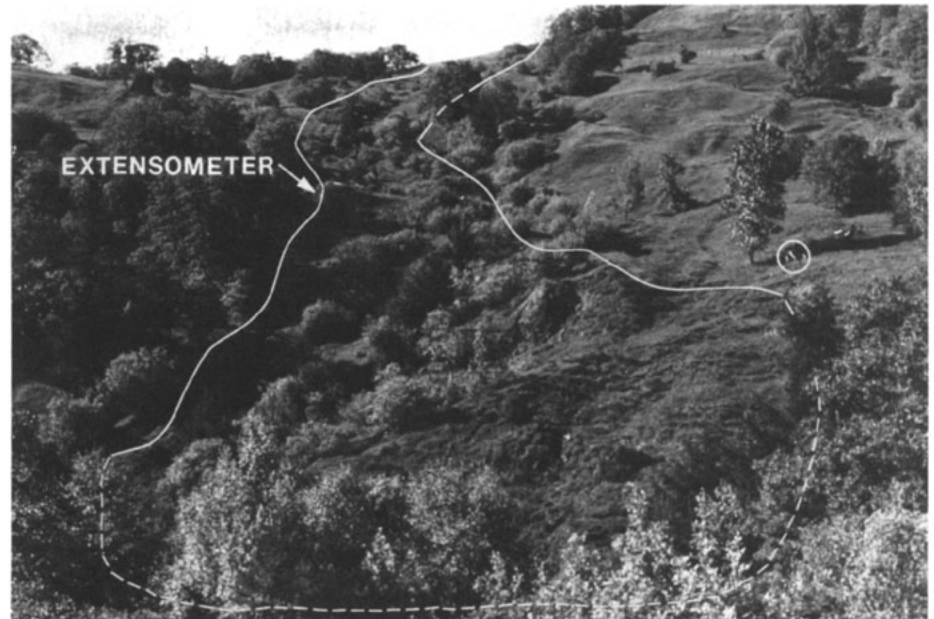


Figure 2. Photograph of typical hummocky surface of Minor Creek landslide in 1982. View is northward from the south side of Minor Creek. The boundary of the main landslide area and the extensometer location are marked. Note horse (circled) for scale.

clusters of willow, poison oak, and blackberry bushes and a few Douglas-fir, oak, and maple trees.

**Characteristics of Landslide Soil**

The physical characteristics of the soil composing Minor Creek landslide were determined from field inspection and laboratory tests of

cores and cuttings collected from about 50 boreholes drilled in 1982. Twelve cores were collected at depths between 3 and 5 m using 4.7-cm-diameter, thin-walled sampling tubes that were hydraulically pressed into the bottoms of cleaned holes; cuttings were collected as they emerged during drilling. The soil characteristics determined for representative core samples are

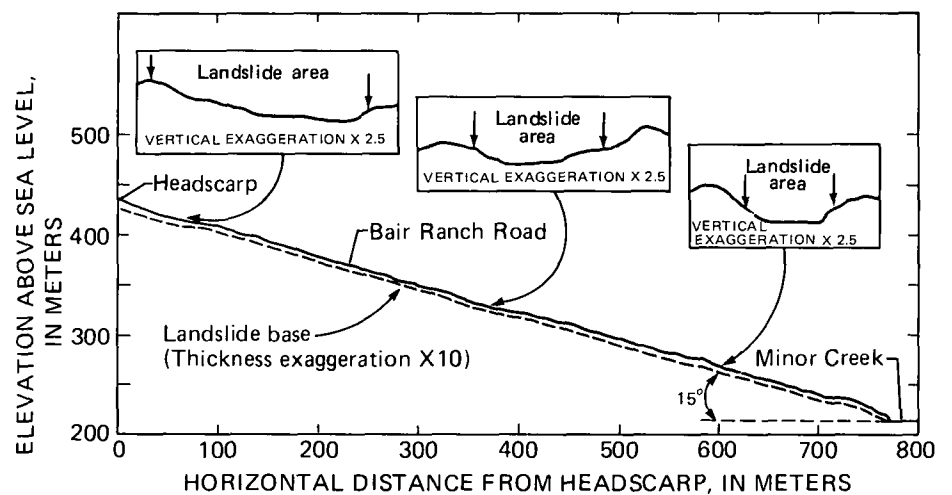


Figure 3. Longitudinal and transverse topographic profiles of Minor Creek landslide. The longitudinal profile is drawn to true scale along the axis of the landslide, but the thickness of the landslide is exaggerated by a factor of 10. Transverse profiles show the topography viewed by an observer facing downslope.

TABLE 1. PHYSICAL CHARACTERISTICS OF SOIL SAMPLES

Bore-hole no.*	Sample depth (m)	Water-table depth (m)	Natural density (kg/m <sup>3</sup> )	Natural water content <sup>§</sup> (wt %)	Dry density (kg/m <sup>3</sup> )	Saturated density (kg/m <sup>3</sup> )	Porosity (%)	Natural soil saturation (% of porosity)	Plastic limit <sup>†</sup> (% water)	Liquid limit <sup>†</sup> (% water)	Plasticity index
44A	3.48	3.54	2197	9.9	1999	2268	26.9	74	15.5	27.4	11.9
44A	4.13	3.54	2208	13.5	1946	2223	27.7	95	15.2	25.0	9.8
44A	4.34	3.54	2108	7.6	1959	2243	28.4	52	8.8	21.8	13.0
45A	3.30	3.17	2165	12.7	1921	2234	31.3	78	13.4	27.0	13.6
45A	3.48	3.17	2152	11.6	1928	2219	29.1	77	20.7	28.5	7.8
45A	3.75	3.17	2144	11.7	1920	2218	29.8	75	18.1	26.4	8.3
mean	3.70	3.36	2162	11.2	1946	2234	28.9	75	15.3	26.0	10.7

\*Bore-hole numbers correspond with piezometer numbers of Figure 5.

<sup>§</sup>Some water was probably lost during sampling, transport, and storage.

<sup>†</sup>Limits were determined using only particles finer than 0.42 mm.

listed in Table 1. Grain-size analyses of the cores indicate the following average weight distribution: 22% gravel, 40% sand, 16% silt, and 22% clay. Overall, the soil is categorized as a poorly sorted, dense, low-plasticity, gravelly clayey sand.

Cores and cuttings also were logged in the field to document soil variations with location and depth. Soil colors varied from browns at the surface to black below depths of from 1 to 6 m, but distinct soil color stratification generally diminished toward the landslide toe. Soil mixing caused by landslide deformation is one of several plausible causes for this downslope color homogenization. We recorded few distinct textural changes with depth, except where drilling met refusal on rock. Refusal on rock may have resulted from contact with "floating boulders" suspended in the soil and may not have reflected stratigraphic boundaries.

Soil within the landslide's basal shear zone appeared the same as the surrounding soil. We attribute this similarity to nearly ubiquitous small-scale foliations, which may be inherited from earlier deformation and which camouflage structural evidence of localized landslide shear. The residual friction angle of the shear-zone soil, inferred from limit-equilibrium analyses of stresses during incipient movement, is between 17° and 18°. Owing to very large strains in the shear zone, we assume that residual cohesion is negligible (compare Mitchell, 1976, p. 313 ff.; Kenney, 1984). We elaborate these strength estimates and our method of limit-equilibrium analysis in the section entitled "Ground Water Effects on Landslide Motion."

#### Landslide Monitoring and Movement

Beginning in 1973, the hydrology, movement, and deformation of Minor Creek landslide have been monitored using a variety of methods

TABLE 2. TYPES OF INSTRUMENTATION AND DURATIONS OF MONITORING AT MINOR CREEK LANDSLIDE

Instrument or method	Quantity	Period of use	Measurement interval	Comments
Recording rain gage	1	1975-	15 minutes	In use
Storage rain gage	1	1974, 1979-	Weekly	In use
Standpipe piezometers (wells)	64	1982-	Weekly	Most in use
Electrical piezometer	1	1982	Continuous	Failed after several months
Electrical piezometer	2	1982	Weekly	Failed after several months
Inclinometer tubes	6	1978-1982	Bimonthly	Became constricted
Inclinometer tubes	9	1982-1984	Bimonthly	Became constricted
Toe extensometer	1	1978-1982	Continuous	Eroded by creek
Lateral extensometer	1	1978-	Continuous	In use
Gully-discharge flumes	2	1979-1982	Continuous	Buried by sediment
Transverse stake lines	5	1973-	Surveyed at least semi-annually	In use
Longitudinal stake line	1	1982-	Surveyed at least semi-annually	In use
Stake strain arrays	10	Various	Surveyed at least semi-annually	Most ruined

Figure 4. Cumulative right-lateral shear displacement measured continuously at the extensometer site (see Figs. 2 and 5) and its relationship to the temporal distribution of rainfall. The extensometer is constructed on stable ground and is wired to a moving point across the lateral shear zone.

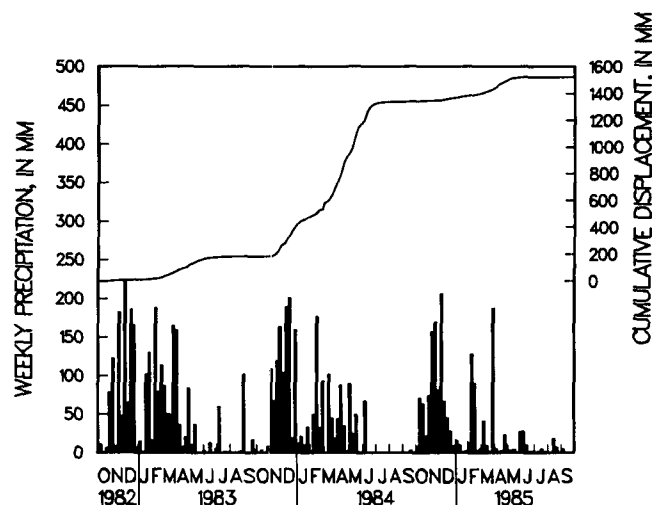


(Table 2; see also Harden and others, 1978; Iverson, 1984, 1985a; Nolan and Janda, in press). Monitoring was most intensive from 1982 to 1985, but relationships shown in Figure 4 between rainfall and landslide movement that were measured from 1982–1985 are broadly representative of the patterns recorded in other years (Iverson, 1984; Nolan and Janda, in press). Typically, the landslide smoothly accelerates sometime between November and March and then maintains a relatively steady pace that is 10 to 100 times faster than its slow summer creep rate of 1 to 4 mm per month. Rapid movement generally persists into May or June, when the landslide smoothly decelerates to its very slow summer rate. Although this pattern is repeated annually, the timing, duration, and speed of movement have no consistent relationship to the timing and amount of rainfall. For example, inconsistent delays between the onset of seasonal rainfall and the onset of rapid movement are shown in Figure 4, and the annual rainfall volume correlates poorly with the duration and speed of movement. Movement also varies from point to point within the landslide (Iverson, 1984, 1985a), but the temporal pattern shown in Figure 4 generally applies throughout.

**Piezometer Installation and Ground-water Data Collection**

Some qualitative insight to the behavior of ground water in Minor Creek landslide was gained during borehole drilling and soil sampling. Most commonly, soil cuttings looked and felt dry and brittle when they emerged from boreholes, even though the holes extended below the water table. The heat generated by the turning auger was apparently sufficient to dry the cuttings, and water flow into the holes was usually so slow that they remained dry unless water was added during drilling. In several instances, however, water flowed rapidly into the boreholes, and the cuttings formed thick slurries. In one case, flow into a borehole was audible. It is apparent, therefore, that widely scattered cracks, conduits, or pronounced high-permeability zones transect the soil in Minor Creek landslide. Compelling evidence for perched water tables is lacking.

To evaluate quantitatively the movement of ground water in Minor Creek landslide, 60 open-standpipe piezometers (hereafter called “wells”) were installed in boreholes throughout most of its length in the summer of 1982; many were installed as nested pairs (Fig. 5). During the summer of 1983, four additional wells were

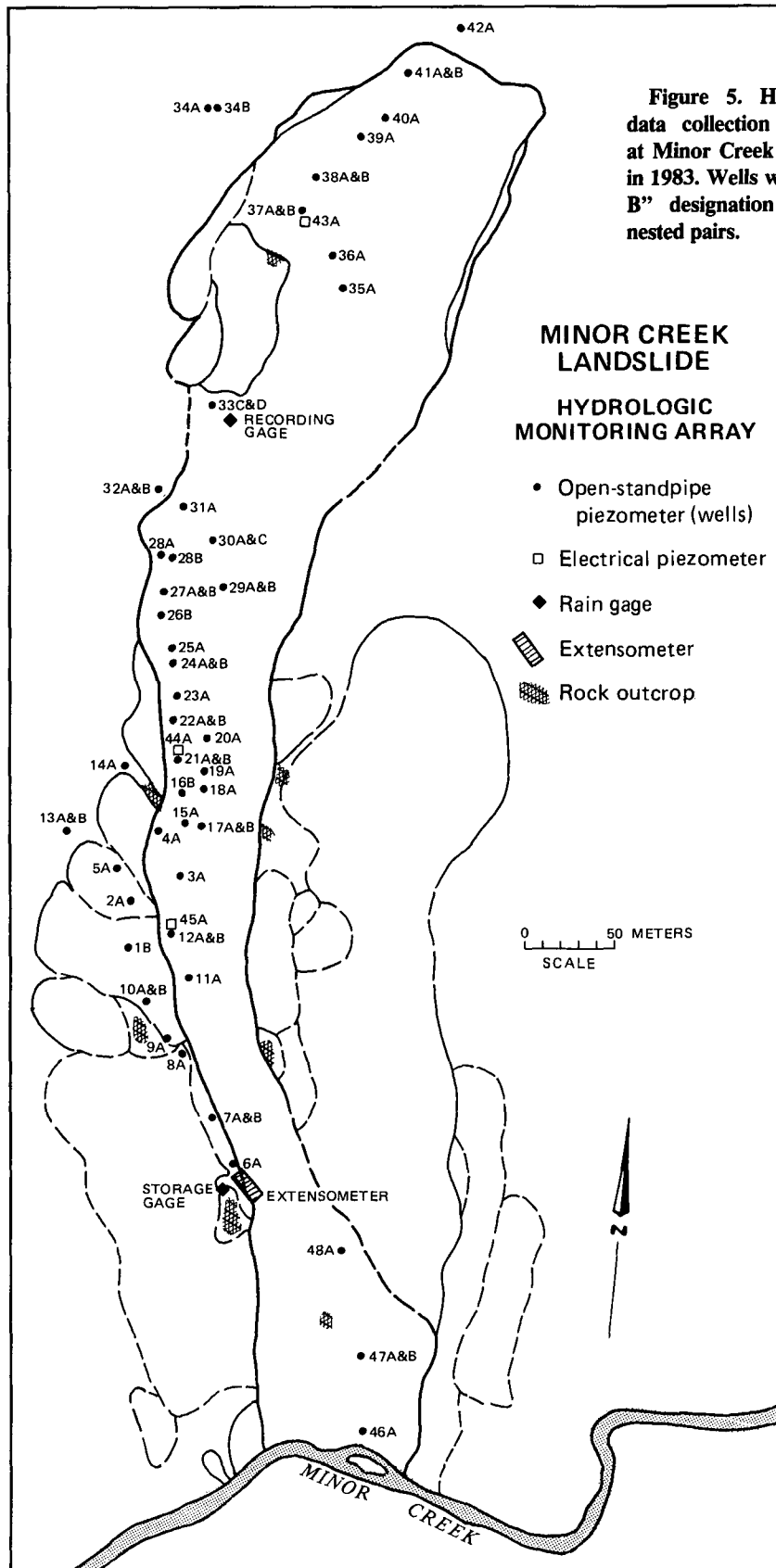


Figure 5. Hydrologic data collection network at Minor Creek landslide in 1983. Wells with “A & B” designation indicate nested pairs.

installed in the toe of the landslide. Construction of the wells is illustrated in Figure 6. Owing to the difficulty of manipulating backfill materials and packing tools at great depths in narrow holes, the quality of well construction typically varied inversely with well depth, which ranged from 1 to 17 m. Water levels in all wells were measured weekly following their installation.

Most of the wells yielded reliable data, although some were poorly constructed, and some failed gradually as they became sheared or plugged. The performance of all wells ultimately was assessed on the basis of installation records and slug-test responses. A well was deemed to yield reliable data if this assessment showed that its construction was good and its characteristic response time (see "Slug Tests" below) was about the same or less than the weekly interval between water-level measurements.

In addition to open wells, three electrical piezometers of the type designed by Wolff and Olsen (1968) were installed in the landslide's basal shear zone. One was connected to a continuous analog recorder. These piezometers, however, began to yield spurious data within a few months of their installation, probably owing to deformation and leakage of the protective housings. Nonetheless, the data collected during the time when both the electrical piezometers and wells were functioning allowed us to compare their responses. On the basis of these comparisons, we concluded that high-frequency head fluctuations that could be missed in the weekly well readings do not occur within the basal shear zone.

### Slug Tests

In the spring of 1985, we conducted slug tests in each of 49 wells through which a probe could pass and in which the perforated casing was wholly below the water table. The objective of the tests was to assess the *in situ* hydraulic conductivity of the surrounding soil and to evaluate well responsiveness and data reliability. In each test, a 500-ml "slug" of water was dropped into the well, and the subsequent rate of water-level decline was recorded. The slug test data were analyzed using the method of Bouwer and Rice (1976), which is based on the theory of steady, radial flow in a homogeneous, porous medium and on well and aquifer geometry. Plots of the slug test data generally yield curves that diverge from theoretical log-linear trajectories after times that range from several seconds to several days (Fig. 7). The log-linear portions of the plots are used to compute values of hydraulic conductivity and  $t_{90}$ , the time necessary for the water level in the well to achieve a 90% response to a change in aquifer head. Table 3 lists well charac-

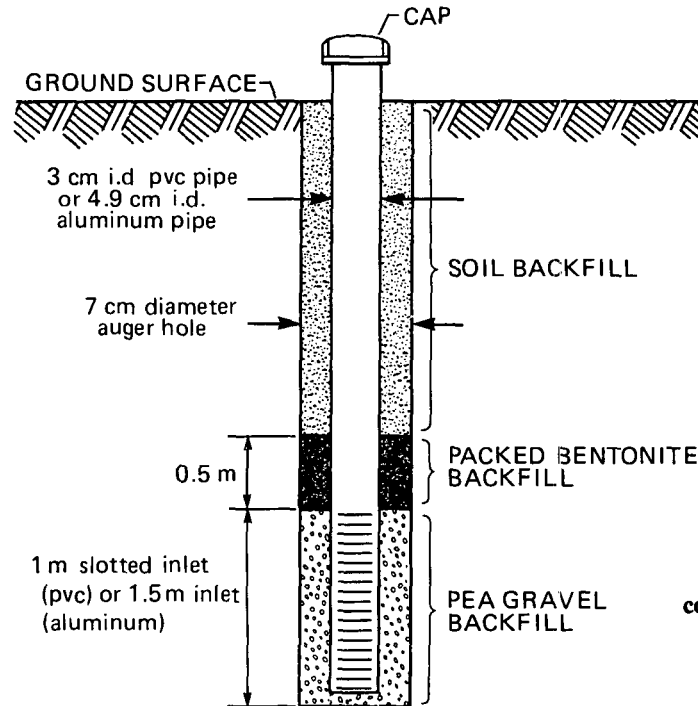


Figure 6. Typical well construction.

teristics and computed conductivities and  $t_{90}$  values obtained from all slug tests that yielded reasonably log-linear responses. Computed conductivities range predominantly from  $10^{-5}$  to  $10^{-9}$  m/s. Twenty-nine wells have  $t_{90}$  response times of 8 days or less, and 27 have  $t_{90}$  response times of 3 days or less. Similar estimates were

obtained for three wells tested in 1982 (Iverson, 1984). Slug tests in some wells, which were apparently plugged or sheared, yielded no response or problematic responses that could not be interpreted quantitatively. These wells were deemed to yield unreliable data.

The value of four wells greater than 4 m deep

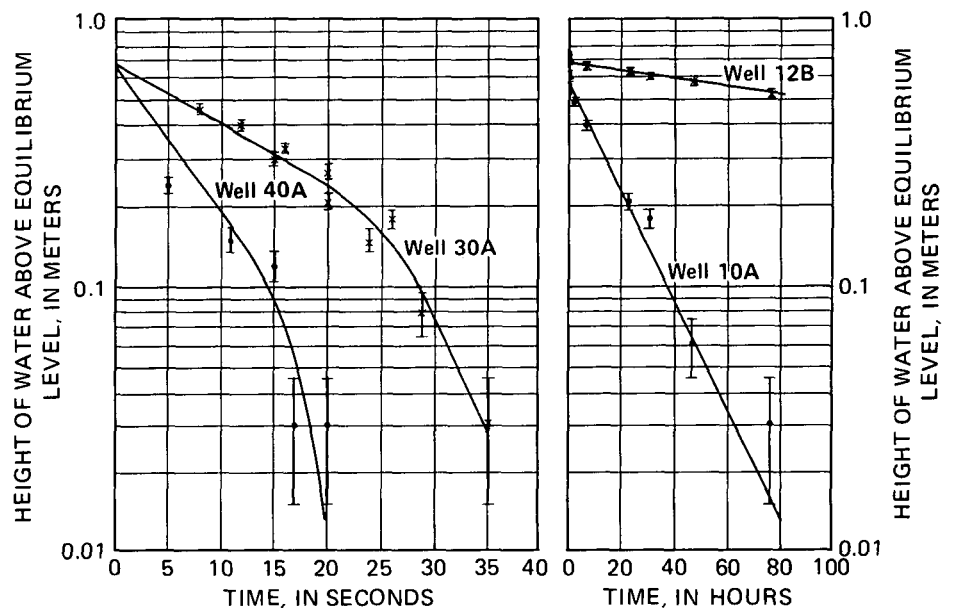


Figure 7. Typical slug-test responses of observation wells, showing response speeds that range from seconds (left diagram) to days (right diagram). Water levels in all wells were read with a precision of  $\pm 0.015$  m. Data plotted on the left diagram were compiled from two tests in each well.

TABLE 3. DEPTHS, HYDRAULIC CONDUCTIVITIES, AND  $t_{90}$  RESPONSE TIMES OF WELLS IN WHICH SUCCESSFUL SLUG TESTS WERE CONDUCTED

Well no.	Well depth (m)	Hydraulic conductivity, $K$ (m/s)	90% response time, $t_{90}$ <sup>†</sup> (d = days)
7A	2.3	$1.3 \times 10^{-8}$	0.5 d
8A	5.4	$3.8 \times 10^{-9}$	3.0 d
10A	1.8	$5.0 \times 10^{-9}$	1.3 d
12B	4.3	$2.5 \times 10^{-10}$	29.1 d
13A	5.4	$1.1 \times 10^{-9}$	7.7 d
13B	2.9	$1.7 \times 10^{-7}$	0.4 d
14A*	5.9	$8.5 \times 10^{-8}$	0.1 d
16B	4.8	$2.6 \times 10^{-8}$	0.3 d
17B	4.1	$6.2 \times 10^{-8}$	0.1 d
18A*	6.3	$8.4 \times 10^{-10}$	15.1 d
20A	4.6	$3.5 \times 10^{-9}$	2.2 d
21A	4.9	$2.7 \times 10^{-10}$	30.8 d
21B	2.4	$1.0 \times 10^{-7}$	0.07 d
22B	3.7	$7.3 \times 10^{-9}$	1.1 d
24B	4.0	$7.5 \times 10^{-8}$	0.1 d
25A	4.8	$1.2 \times 10^{-8}$	0.7 d
27B	3.6	$5.1 \times 10^{-8}$	0.2 d
28A	3.3	$3.6 \times 10^{-8}$	0.2 d
28B*	7.7	$4.4 \times 10^{-7}$	0.03 d
29B	3.6	$1.6 \times 10^{-7}$	0.05 d
30A	8.1	$1.6 \times 10^{-5}$	45 s
30C	3.1	$8.3 \times 10^{-8}$	0.1 d
31A	9.2	$3.0 \times 10^{-10}$	24.4 d
32A	6.8	$4.6 \times 10^{-9}$	1.5 d
32B	1.9	$2.3 \times 10^{-8}$	0.2 d
34A	2.9	$2.5 \times 10^{-7}$	0.03 d
37A	6.9	$2.4 \times 10^{-8}$	0.4 d
37B	3.3	$3.3 \times 10^{-8}$	0.2 d
38A	7.1	$1.2 \times 10^{-9}$	8.0 d
38B	2.7	$1.5 \times 10^{-7}$	0.05 d
40A	4.3	$3.3 \times 10^{-5}$	18 s
41B	2.8	$1.2 \times 10^{-7}$	0.05 d

\*Aluminum tube; tubes not marked are PVC.

<sup>†</sup> $t_{90}$  was calculated using equation 11 of Bouwer and Rice (1976), but with  $t_{90}$  occurring when  $y = 0.1 y_0$ , not  $0.9 y_0$ .

for measuring changes in ground-water head is questionable because they have  $t_{90}$  values significantly greater than one week (Table 3). A difficulty arises in interpreting these large  $t_{90}$  values, because it is unclear whether they reflect low *in situ* conductivity, poor well installation, or both. For purposes of further analysis, therefore, only wells that yielded  $t_{90}$  values of 8 days or less (that is, approximately the time interval between

head measurements) will be considered. For these wells, Figure 8 shows the lack of a significant correlation between hydraulic conductivity and well depth. In our subsequent analyses, we therefore regard well responsiveness as independent of depth. Three very responsive wells (12A, 34B, and 42A) that could not be slug tested owing to low water levels will also be considered in our analyses.

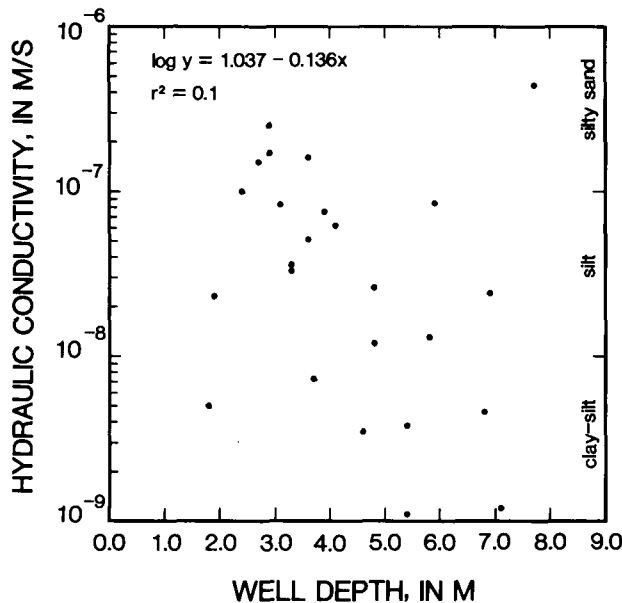


Figure 8. Scatter plot of hydraulic conductivity as a function of well depth for all wells with a  $t_{90}$  response time of 8 days or less. The regression equation and coefficient of determination indicate little correlation. Typical soil textures that correspond to the range of measured hydraulic conductivities are shown for reference, and are taken from Freeze and Cherry (1979, p. 29).

One notable exception to the typical pattern of well behavior exists. Well 18A is more than 6 m deep and yielded a very low hydraulic conductivity estimate ( $K = 10^{-10}$  m/s,  $t_{90} = 15$  days), yet it responded sharply to rainfall (Fig. 9f). This well may be close to a deep crack or conduit that fills rapidly with water during storms but is not affected by slug tests. Owing to its highly anomalous behavior, well 18A will not be included in our quantitative analyses.

ANALYSIS OF GROUND-WATER FLOW

Qualitative Inferences from Field Data

Rainfall and reliable ground-water data collected during water years 1983, 1984, and 1985 are summarized in Figure 9. (Water years end on September 30 of the corresponding calendar year.) Total rainfall during these water years was 2,674 mm, 2,143 mm, and 1,638 mm, respectively. Despite marked differences in the amount and distribution of rainfall, the seasonal responses of water levels in most wells were remarkably consistent from year to year (Fig. 9). Differing responses were, however, measured at different points in the landslide. These spatial differences accurately reflect spatial variations in ground-water responses, because the differences cannot be attributed to significant differences in  $t_{90}$  well-response times.

Important spatial and temporal patterns become evident when the water-level responses (that is, hydrographs) of Figure 9 are compared systematically. Figure 10 facilitates one such comparison by depicting the mean hydrographs calculated for wells grouped according to depth. The figure shows that hydraulic heads tend to be higher in shallow wells (<3 m deep) than in intermediate (3 to 6 m deep) or deep wells (>6 m deep). This indicates that a downward component of the hydraulic gradient persists year-long throughout most of the landslide, and that deep portions of the ground-water flow field are continuously recharged by percolation from above.

Water levels measured in most wells are strongly modulated about high, wet-season levels (Figs. 9 and 10). After a seasonal high level is reached, it tends to be quite perseverant and is affected relatively little by superposed short-term fluctuations. Virtually all wet-season water levels in shallow wells are less than 1 m below the ground surface, and many are within a few decimetres of the surface. We therefore infer that the landslide is almost completely saturated during most of the rainy season.

The amplitudes and shapes of the hydrographs of Figures 9 and 10 provide evidence of

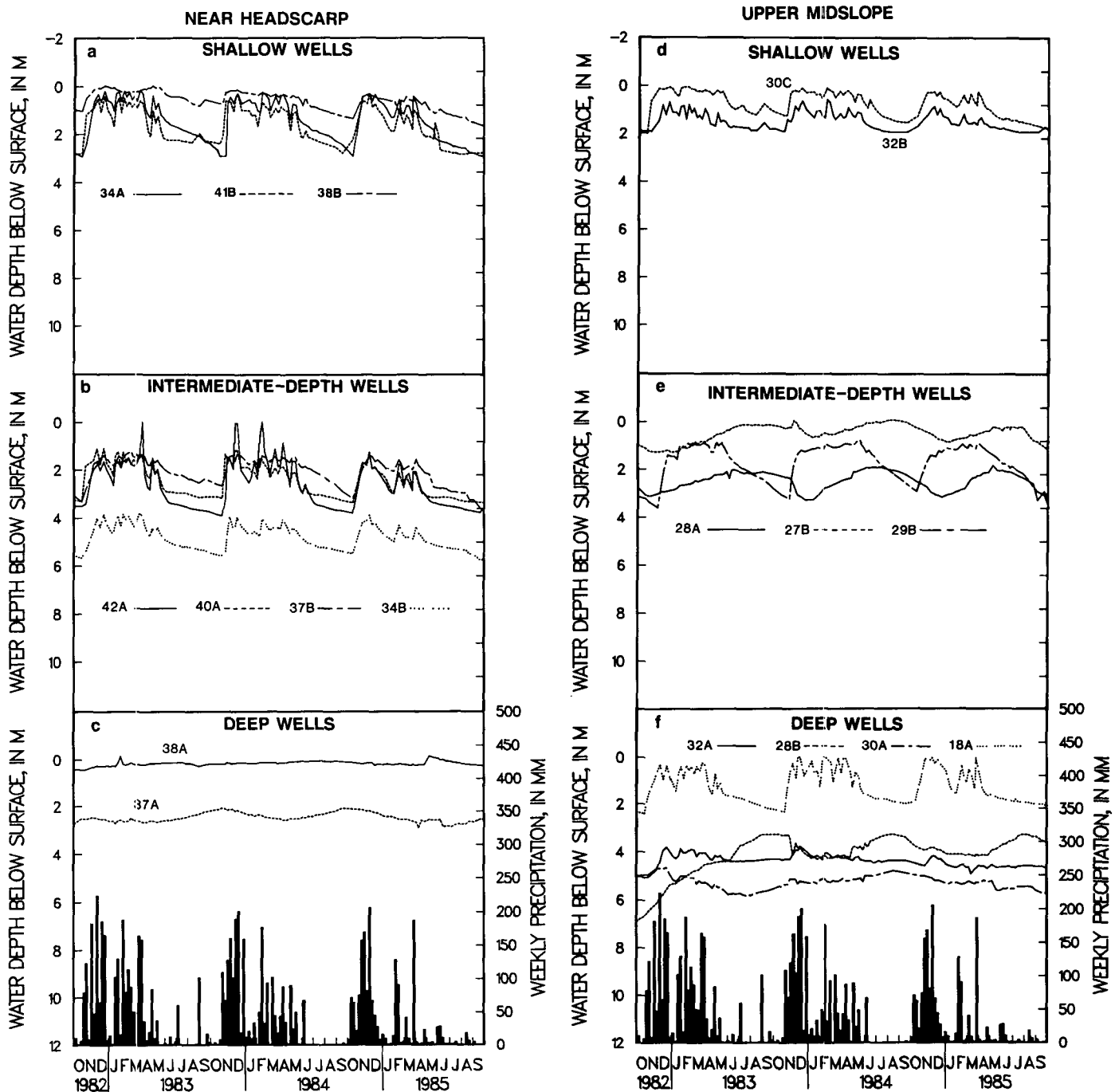


Figure 9. Weekly rainfall histograms and ground-water hydrographs for all wells with  $t_{90}$  response times of 8 days or less (except for well 18A) for water years 1983, 1984, and 1985. Numbers refer to individual wells (compare Fig. 5). The hydrographs are grouped according to well location and depth; shallow wells are less than 3 m deep; intermediate-depth wells, 3 to 6 m deep; and deep wells, 6 to 9 m deep. Each year between midsummer and the onset of the following rainy season, wells 42A, 10A, 12A, and 13B usually were dry. Hydrographs for these wells during the dry periods were estimated on the basis of data from nearby wells.

how rainfall recharges the landslide's ground-water flow field. The hydrographs of shallow wells typically reflect large, abrupt head increases during the onset of the rainy season and gradual drainage at the end. During the early rainy season in November 1983, head increases were particularly abrupt, and the measured rainfall volume was less than one-third the empty pore volume that would have to fill to account

for the measured water-table rise (see Appendix)<sup>1</sup>. This disproportionate rise was apparently caused by unusually abundant rain during the previous dry season, which helped to sustain a thick zone of nearly saturated soil that saturated

<sup>1</sup>The Appendix may be obtained from the GSA Data Repository free of charge. Request Supplementary Data 87-24 from the GSA Documents Secretary.

quickly during the November rains (compare Gillham, 1984). Despite this type of influence on seasonal responses, dry-season rains generally cause little direct recharge of the saturated zone, as shown by their insignificant effect on hydrographs. During the wet season, in contrast, weekly rainfall cycles cause sharp fluctuations in hydrographs of shallow wells, reflecting nearly complete saturation of the landslide and

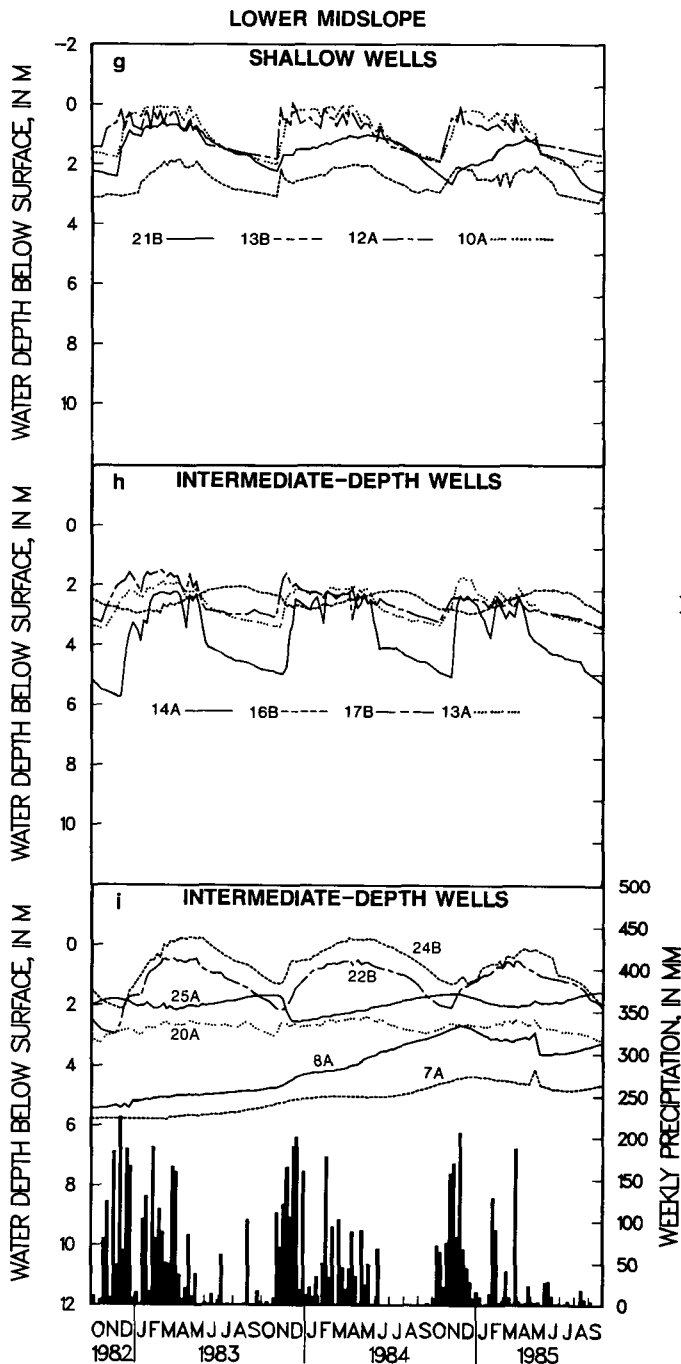


Figure 9. (Continued).

those of wells adjacent to its margins (see Fig. 5). All wells off the landslide (13a, 13b, 14a, 32a, 32b, 34a, 34b, and 42a) show clear responses to weekly, wet-season rainfall cycles, with little attenuation or lag (Fig. 9). Four of these wells (13a, 14a, 32a, and 34b) are more than 5 m deep, and the lack of significant response attenuation at this depth leads us to hypothesize that soil outside the landslide may be more structured than that within the landslide. Pervasive networks of millimetre-scale soil cracks that allow rapid percolation from the surface may be destroyed by landslide movement and soil mixing. Ground-water responses could hence become more attenuated as a result of movement. Furthermore, the most responsive intermediate-depth wells in the landslide are those located near the headscarp (Fig. 9), where soil displacement and disruption have been least. The hypothesis that soil is disrupted as it travels downslope is consistent with evidence that soil stratification is least distinct in the lower part of the landslide.

Ground-water heads in one part of the landslide indicate the presence of a flow cell. In the area between wells 21 and 24 (Fig. 5), heads commonly increase with increasing well depth (Figs. 9g, 9h), showing that an upward component of ground-water flow exists. Moreover, in a somewhat larger area between wells 16 and 28 (Fig. 5), nearly all wells have smooth seasonal hydrograph peaks that lag behind the seasonal rainfall by at least a few months (Fig. 9). For shallow wells, the lag is unique to this area, and it indicates that most ground water in this area probably infiltrated elsewhere, subsequently reaching the wells via lateral and upward flow. Local upflow could be caused by a subsurface shelf of coherent rock that may extend between outcrops mapped on either edge of the landslide near well 18 (Fig. 5). This is the only part of the landslide where augering encountered rock at a consistent depth, about 6 to 8 m. An alternative or attendant explanation for the upflow is that the ground-water flow system is locally influenced by microtopography, so that elevation contrasts drive flow cells that include adjacent zones of upward and downward flow. Ground-water circulation driven by elevation contrasts can be assessed conceptually by considering the theory of steady, Darcian potential flow.

**Inferences from the Theory of Steady Darcian Potential Flow**

As noted above, ground-water heads at Minor Creek landslide exhibit relatively minor temporal variation during the wet season, and water levels in shallow wells closely follow the ground surface. We therefore infer that the landslide is virtually saturated during the wet season and that ground-water flow is driven predominantly by elevation contrasts. Although

rapid recharge at shallow depths. Intermediate-depth wells generally show more attenuated, slower, wet-season responses, indicating that water fluxes from rainfall diffuse somewhat before reaching this depth. Deep wells normally have very subdued hydrographs, and the mean response lags behind the rainfall by nearly nine months.

The greater attenuation of mean hydrograph amplitudes at greater well depths, as shown in Figure 10, appears to be authentic and is not an artifact of data averaging. A mean hydrograph for a group of wells could show fictitious attenuation or smoothing if the response variability

between wells were significantly time-dependent. We found, however, that independent of the date on which measurements were made, the standard deviation about the mean head for a group of wells is nearly constant. For the shallow wells, the deviation is about 0.8 m, whereas it is about 1.6 m for the intermediate wells and 2.0 m for the deep wells. Thus despite head variability that increases with well depth, the envelope of statistically expected hydrographs for a particular well depth has nearly the same shape as the mean hydrograph for that depth.

Some distinction can be drawn between the hydrographs of wells on the landslide versus

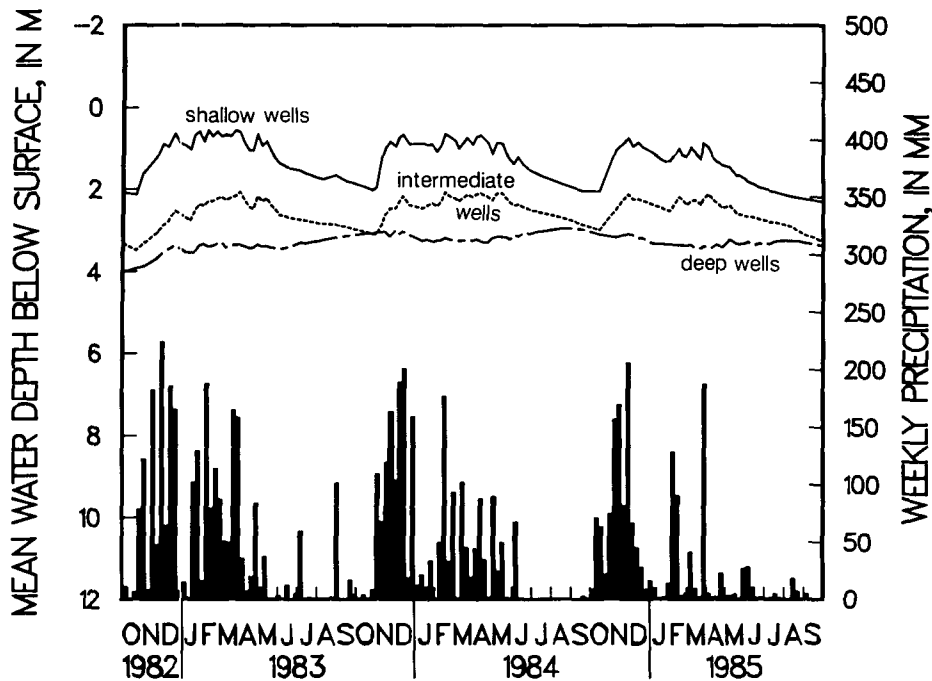


Figure 10. Mean hydrographs for the shallow, intermediate, and deep wells computed from the hydrographs shown in Figure 9 (excluding well 18A).

soil deformation may alter the hydraulic head distribution, we have observed no head fluctuations that clearly were caused by landslide movement. We thus assume that the soil deforms with constant volume and that deformation effects may be neglected (compare Iverson, 1985b, 1986b). We analyze simple but important features of the mean, wet-season groundwater flow field by assuming steady, gravity-driven, Darcian potential flow in a saturated, homogeneous, isotropic, porous slope.

As a first step in our analysis, we construct a simple, quantitative flow net that shows the mean, wet-season groundwater head distribution in an ideal, uniform cross section of part of the landslide (Fig. 11). The flow net is constrained by the mean slope of the water table, which gives  $\partial(\text{head})/\partial x = -\partial y/\partial x = -\sin 15^\circ$ , and by the wet-season well data of Figure 10, which give  $\partial(\text{head})/\partial y = -0.6$ . Here  $y$  is a vertical coordinate measured downward from the ground surface, and  $x$  is a coordinate parallel to the surface. No basal or lateral flow boundaries are imposed. The flow net shows that, on average, wet-season groundwater flow is driven by a total head gradient of magnitude 0.6 to 0.7, which includes a strong vertically downward component. The downward component of flow reflects widespread infiltration and recharge, and it affects the balance of forces that controls landslide motion.

We next consider the complicating hydrogeologic effects of the hummocky landslide surface. We use numerical model results to illustrate how ground water flows in ideal, saturated hillslopes on which sinusoidal microtopography is superimposed. Toth's (1963) analytical work first clarified the role of various scales of topography in driving steady, saturated groundwater flow, and Freeze and Witherspoon (1966, 1967) used numerical models to elaborate the results. All of these studies, however, treated only slopes with inclinations less than about  $5^\circ$  and with horizontal basal flow boundaries. Here we present results from models similar to those of Freeze and Witherspoon (1966), extended to consider steeper slopes and sloping basal flow boundaries.

Figure 12 shows flow nets that represent numerical solutions for steady, two-dimensional flow in a hummocky slope with a mean inclination of  $15^\circ$ . The head at each point on the sinusoidal slope surface is set equal to the point's elevation above a horizontal datum, thus providing the driving force for groundwater flow. Zero-flux boundaries along the lateral flow margins represent topographic groundwater divides. A basal zero-flux boundary is placed parallel to the mean ground surface at three trial depths, because the true boundary depth is un-

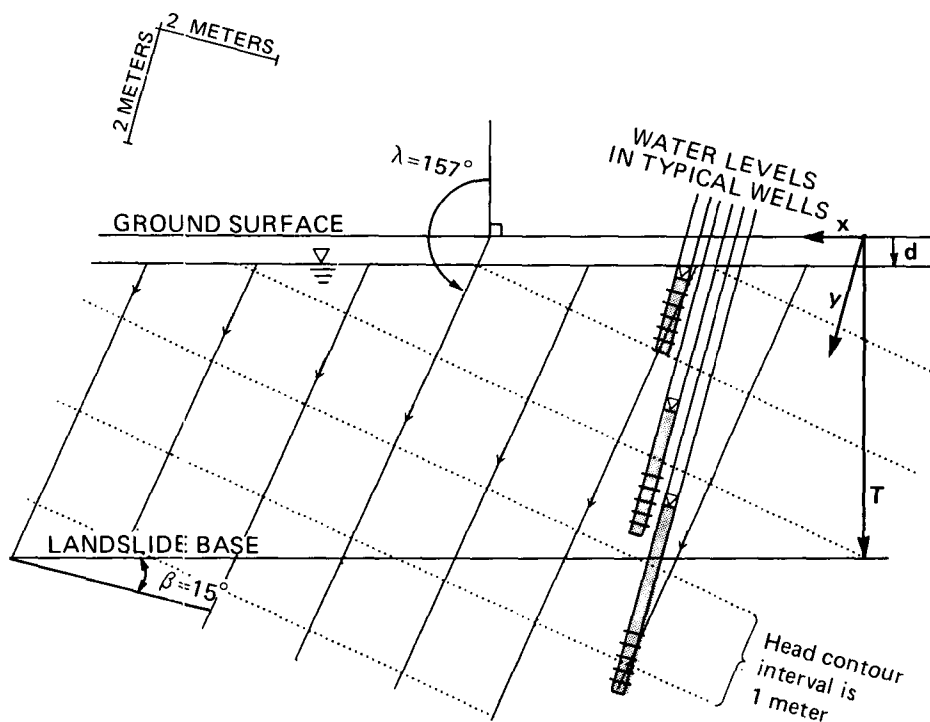


Figure 11. Quantitative, empirical flow net showing the average wet-season groundwater flow field in Minor Creek landslide. The flow net is inferred from the mean water-table slope and mean water levels in shallow, intermediate, and deep wells, and the flow field is assumed to be uniform. Dotted lines represent head contours (equipotentials), and solid lines represent seepage vectors (streamlines). Geometric quantities used for limit-equilibrium stability analyses are defined.

known. We infer, however, from the weathered-mantle origin of the soil at Minor Creek landslide and from seismic refraction studies (Bromirski and Dengler, 1985) that a relatively impermeable boundary probably exists subparallel to the ground surface.

Figure 12 demonstrates schematically that ground water circulates in cells of differing size in a steep, saturated, soil-mantled hillslope with hummocky microtopography. These different scales of circulation are for our purposes designated the "hillslope scale" [conceptually similar to Toth's (1963) regional scale] and the "local

scale." Ground water circulates on the hillslope scale owing to recharge near the top of the slope and discharge near the base. Local-scale circulation results from hydraulic gradients caused by the surficial hummocks and is most conspicuous where large-scale recharge and discharge do not overwhelm the local flow. Local flow in a direction contrary to the hillslope flow is suppressed by the over-all steepness of the slope. Interest-

ingly, both local recharge and discharge are concentrated in the concavities that separate hummocks, with discharge focused near the bases of steep sections of the slope.

Figure 12 also shows that local ground-water circulation can extend to considerable depths throughout much of the hillslope, regardless of the lower, impermeable boundary depth. The depth of local flow cells, that is, the depth to which local flow paths descend before returning to the adjacent ground surface, is about five times the amplitude of the sinusoidal microtopography. Additional simulations show that this "factor-of-five" estimate also applies for other microtopographic amplitudes if the average surface slope is 15°, with relatively little dependence on the microtopographic wavelength or the lower flow boundary depth. Thus, irrespective of the particular pattern of the microtopography, it can significantly influence ground-water flow in steep, saturated slopes. The influence may be seen at a few places on Minor Creek landslide, where springs discharge near the bases of steep hummock faces. Kelsey (1978) has made similar observations on other landslides nearby, and Cooley (1983) and Winter (1983) have shown that similar, albeit more complex, flow-cell phenomena are predicted theoretically if one considers the effects of transient and unsaturated flow.

#### Inferences from the Theory of Transient Vertical Flow

Interpreting the time-dependent head fluctuations shown in Figures 9 and 10 requires that we augment the steady-state flow analysis with another approach. A simple theory of transient, vertical ground-water flow provides a straightforward means of interpreting the head fluctuations. This approach is justified because where recharge occurs, its dominant component is directed vertically downward (Figs. 11 and 12). Understanding recharge and head fluctuations is, of course, very important for understanding the changes in effective stress that cause seasonal landslide motion.

We employ a very simple model of transient, vertical ground-water flow—a model based on the linear diffusion equation. Our aim is to show that this model explains many of the important features of the ground-water head fluctuations measured at Minor Creek landslide. Vertical, transient, Darcian flow of an incompressible, homogeneous liquid in a homogeneous, one-dimensional, linearly elastic porous medium that is not subject to external loading is expressed by the diffusion equation (Gambolati, 1973):

$$\frac{\partial p}{\partial t} = C \frac{\partial^2 p}{\partial y^2} \quad (1)$$

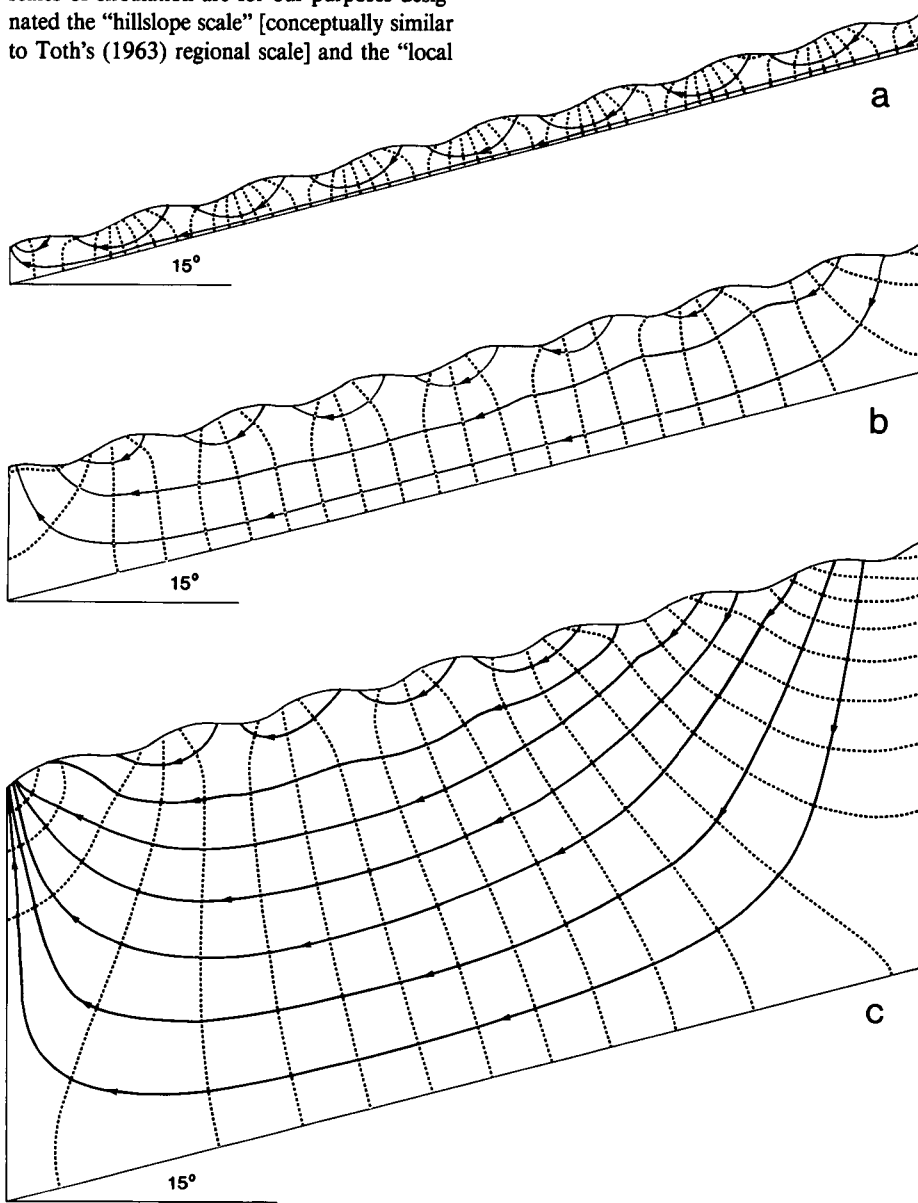


Figure 12. Flow nets generated from numerical simulations of steady, two-dimensional ground-water flow in saturated, homogeneous, isotropic hillslopes with a mean slope of 15° and sinusoidal microtopography (hummocks) on the surface. Dotted lines represent equipotentials, and solid lines represent streamlines. No distortion of the horizontal or vertical scales is used. In each flow net, the ratio of the sinusoidal hummock amplitude to the slope length is 1:60, corresponding to 5-m-high hummocks at Minor Creek landslide. The mean depth of the impermeable basal flow boundary varies by a factor of 10 between diagrams a and c.

in which  $p$  is pore-water pressure head,  $t$  is time,  $y$  is vertical depth below the ground surface, and  $C$  is hydraulic diffusivity. Elevation changes due to soil deformation are assumed negligible, and  $p$  wholly represents the transient component of the total hydraulic head. The assumptions involved in deriving equation 1 from the considerably more rigorous unsaturated-saturated flow equation of Narasimhan (1982), as well as an explanation of the physical meaning of  $C$  for unsaturated-saturated flow, are presented in detail in the Appendix. Briefly,  $C$  is equal to the hydraulic conductivity of the soil,  $K$ , divided by the storage parameter  $\partial\theta/\partial p$ , where  $\theta$  represents the volumetric water content of the soil. The linearity of the diffusion equation depends on the assumption that  $C$  is a global constant, which is most nearly satisfied when the landslide soil is saturated (compare Eagleson, 1970, p. 291–295). The assumption consequently is best for analyzing wet-season ground-water head fluctuations and is poorest for understanding detailed behavior during the dry season.

We consider a solution of equation 1 that shows how pore-pressure waves that result from periodic rainfall travel downward from the ground surface. The pressure waves should not be confused with acoustic waves—they are primarily a manifestation of ground-water mass flux and not of elastic energy transmission. To investigate the effects of rainy periods of any intensity and duration, we analyze the propagation and attenuation of the waves over an unconstrained range of amplitudes and frequencies. Appropriate boundary conditions stipulate that the pore pressure varies sinusoidally at the ground surface (where  $y = 0$ ) with some amplitude  $p_0$  and some frequency  $n$ , and subsurface pore pressures are unconstrained except that their change becomes negligible at an infinite depth. Mathematically these conditions are stated as:

$$p(0, t > 0) = p_0 \cos(2\pi nt) \quad (2a)$$

$$\frac{\partial p}{\partial y}(\infty, t) = 0 \quad (2b)$$

The initial condition stipulates a steady distribution of pressure:

$$p(y, 0) = p_{\text{steady}} \quad (2c)$$

The solution of the problem posed by equations 1 and 2 consists of the sum of a sinusoidally fluctuating term and a decaying term that reflects the arbitrary initial pressure,  $p_{\text{steady}}$  (Carslaw and Jaeger, 1959, p. 64–65). Here we are concerned only with the effects of the pressure fluctuations that result from rainfall variations. The

fluctuating part of the solution is adapted from the analogous heat-conduction solution given by Carslaw and Jaeger:

$$\frac{p}{p_0} = \exp[-y(n\pi/C)^{1/2}] \cdot \cos[2\pi nt - y(n\pi/C)^{1/2}] \quad (3)$$

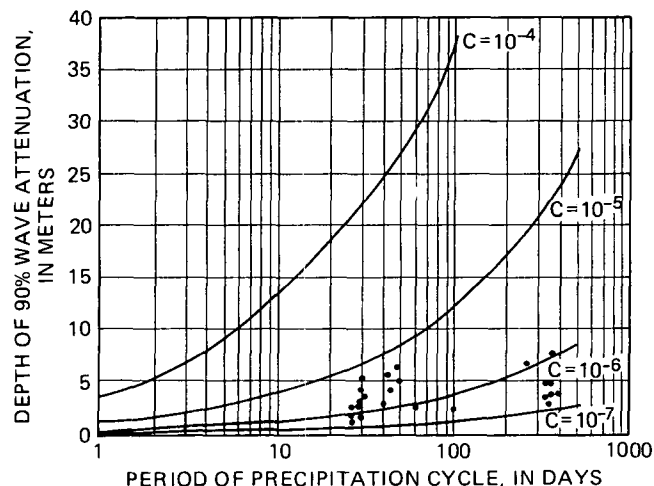
Equation 3 represents the propagation of an attenuating pore-pressure wave of speed  $(4n\pi C)^{1/2}$ , wavelength  $(4\pi C/n)^{1/2}$ , and frequency  $n$ . Carslaw and Jaeger (1959, p. 66–70) present a detailed mathematical discussion and dimensionless plots of equation 3. They show that if the sinusoidal pressure-wave boundary condition enforced at the ground surface (that is, equation 2a) is replaced by a square wave (perhaps a better simulation of rainfall input), it affects the solution little because square waves degenerate into sinusoids over a short travel distance. Furthermore, they show (p. 75–76) that if the water flux instead of pressure varies sinusoidally at the surface, it produces essentially the same result as equation 3, although a flux boundary makes the wave amplitude vary in a more complicated manner. Here we neglect such complicated amplitude variations to focus on the essential features of pressure-wave propagation.

Equation 3 shows how the duration of rainfall cycles and the hydraulic diffusivity of the soil control the (1) amplitude, (2) speed, and (3) phase delay of pore-pressure responses at depth. (1) The amplitudes of the pressure waves attenuate exponentially as water descends into the soil. The attenuation factor is given by  $\exp[-y(n\pi/C)^{1/2}]$ , meaning that high-frequency waves attenuate the most dramatically. Attenuation is enhanced by low diffusivities, which are associated with low hydraulic conductivities or high ground-water storage capacities. The theo-

retical depths at which pressure waves attenuate to 10% of their surface amplitude are plotted on Figure 13 as a function of the period of rainfall cycles and the magnitude of the diffusivity. (2) High-frequency pressure waves travel faster than do low-frequency waves. The wave speed is increased by increasing the hydraulic diffusivity. (3) A progressive phase lag of time duration  $y(\pi/nC)^{1/2}$  affects the wave propagation and is derived from the argument of the cosine function in equation 3. Depth is the dominant factor affecting both phase lag and attenuation, because it enters both terms linearly. The over-all picture derived from equation 3 is that at shallow depths one would expect to observe the effects of high-frequency pressure waves with relatively little attenuation or delay following rainfall; at great depths, the high-frequency waves would not be distinguishable, and one would expect to observe only slow, low-frequency waves that lag behind the rainfall cycle.

To compare the quantitative predictions of equation 3 with our data, we need to estimate a representative value of the hydraulic diffusivity,  $K/(\partial\theta/\partial p)$ . Hydraulic conductivities measured at Minor Creek landslide are approximately log-normally distributed (Fig. 8), so that a representative value is the geometric mean,  $K = 5 \times 10^{-8}$  m/s. A representative value of the storage parameter  $\partial\theta/\partial p$  is more problematic, because ideally it should reflect a combination of saturated-unsaturated storage and soil consolidation and swelling during both drainage and recharge. The typical variability of storage parameters, however, is considerably less than that of hydraulic conductivities (Freeze and Cherry, 1979, p. 58–62). On the basis of our knowledge of soil composition and our estimates of specific yields during seasonal water-table rises (Appen-

**Figure 13. Curves showing theoretical depth of 90% pore-pressure wave attenuation as a function of the precipitation-cycle period for various values of the hydraulic diffusivity,  $C$ , expressed in  $\text{m}^2/\text{s}$ . Field data are shown as plotted points; the ordinate represents well depth, and the abscissa represents the shortest distinguishable period of water-level fluctuation in the well.**



dix), we can confidently estimate that a storage parameter value of  $5 \times 10^{-2} m^{-1}$  is accurate within a factor of ten (compare Freeze and Cherry, 1979, p. 61; Bear, 1979, p. 88). Consequently, we estimate that a representative hydraulic diffusivity is about  $10^{-6} m^2/s$ .

To compare our data with diffusion-theory predictions of pressure-wave attenuation, we measured the shortest distinguishable wavelengths on each hydrograph shown in Figure 9. We assume that the shortest distinguishable wavelengths represent the frequencies of rainfall effects that are ~90% attenuated at each well's depth. The wave period corresponding to the mean of these short wavelengths for each hydrograph is the abscissa of the data points plotted on Figure 13, and the well depth is the ordinate. The data show that high-frequency (short-period) pressure waves generally attenuate at shallower depths than do low-frequency waves, in agreement with theory. They also show that a hydraulic diffusivity of the order of  $10^{-6} m^2/s$  predicts wave attenuation reasonably well (Fig. 13). This independent estimate agrees quantitatively with the diffusivity estimated from the hydraulic conductivity. Adopting this diffusivity value, the theory predicts 90% attenuation of weekly waves at a depth of 1.0 m, 90% attenuation of 2-month waves at a depth of 3.0 m, and 90% attenuation of annual waves at a depth of 7.3 m (Table 4). These three classes of wave attenuation therefore represent our physical interpretation of the mean temporal behavior of hydraulic heads measured in shallow wells, intermediate wells, and deep wells in Minor Creek landslide. That is, heads in shallow wells reflect the influence of every storm, within the resolution of our weekly measurements. Heads in intermediate wells are less sensitive to individual storms but respond to rainfall on a month-to-month basis. In deep wells, heads re-

TABLE 4. PROPAGATION PROPERTIES OF PORE-PRESSURE WAVES FOR DIFFERENT FREQUENCIES OF RAINFALL CYCLES

Frequency (n)	Wave length ( $4\pi C/n$ ) <sup>1/2</sup>	Wave speed ( $4\pi nC$ ) <sup>1/2</sup>	90% attenuation depth, $y_{90}$	Phase lag at $y_{90}$ $y_{90}(\pi/nC)$ <sup>1/2</sup>
$1.65 \times 10^{-6}/s$ (1/n = 1 week)	2.8 m	$4.6 \times 10^{-6} m/s$ (2.8 m/week)	1.0 m	$2.2 \times 10^5 s$ (2.5 days)
$1.90 \times 10^{-7}/s$ (1/n = 2 months)	8.1 m	$1.5 \times 10^{-6} m/s$ (0.94 m/week)	3.0 m	$1.9 \times 10^6 s$ (22 days)
$3.17 \times 10^{-8}/s$ (1/n = 1 yr)	20.0 m	$6.3 \times 10^{-7} m/s$ (0.38 m/week)	7.3 m	$1.1 \times 10^7 s$ (130 days)

Note: a hydraulic diffusivity of  $10^{-6} m^2/s$  is assumed.

flect little other than seasonal or longer term rainfall cycles.

The wave speed, length, and phase lag associated with different wave frequencies can also be calculated using the  $10^{-6} m^2/s$  diffusivity estimate (Table 4). The calculations show that all pore-pressure waves attenuate almost completely before they have traveled more than half a wavelength into the soil. Consequently, oscillatory pressure distributions, in which a zone of high pressure is overlain and underlain by low-pressure zones, would be unlikely to occur. The calculated phase lags at the depth of 90% wave attenuation range from 2.5 days for weekly cycle waves to 130 days for annual cycle waves. Ground-water responses at the landslide base are thus predicted to lag a few weeks to a few months behind the rainfall cycle. This prediction generally corresponds well with our field data (Figs. 9 and 10).

**GROUND-WATER EFFECTS ON LANDSLIDE MOTION**

Temporal and spatial variations in ground-water flow influence the effective stress distribution and motion of Minor Creek landslide in several ways. Effects of temporal flow variations are perhaps more obvious and are discussed first.

**Temporally Variable Flow and Instigation of Motion**

Times of high ground-water head at the base of Minor Creek landslide correspond well with times of rapid landslide motion (Fig. 14). The horizontal line in Figure 14 shows that whenever rapid motion occurs, a critical water level is exceeded in intermediate-depth wells. This critical water-level line nearly coincides with seasonal hydrograph peaks, so that the head distribution that triggers rapid motion is nearly the same as the perseverant, wet-season head distribution that exists when the landslide is almost saturated.

The critical water level of Figure 14 probably surpasses any rainfall parameter as an accurate predictor of the timing of landslide motion. In 1983, for example, seasonal motion commenced in early November, the earliest of any documented year, despite antecedent rainfall that was less than in the preceding or following years. We infer that the early motion was due to unusually great ground-water storage in the unsaturated zone, which led to the anomalously abrupt water-table rise early in the 1983-1984 rainy season. The rapid water-table rise soon led to increased heads at the landslide base, as water diffused downward from the surface and heads assumed their perseverant wet-season distribution.

Seasonal landslide motion triggered by changes in the ground-water head distribution can be analyzed with a simple, limit-equilibrium model of infinite slopes. This model employs a balance between driving and resisting forces to calculate the stress state for incipient motion in a planar slope of infinite areal extent. Minor Creek landslide is very long and wide relative to

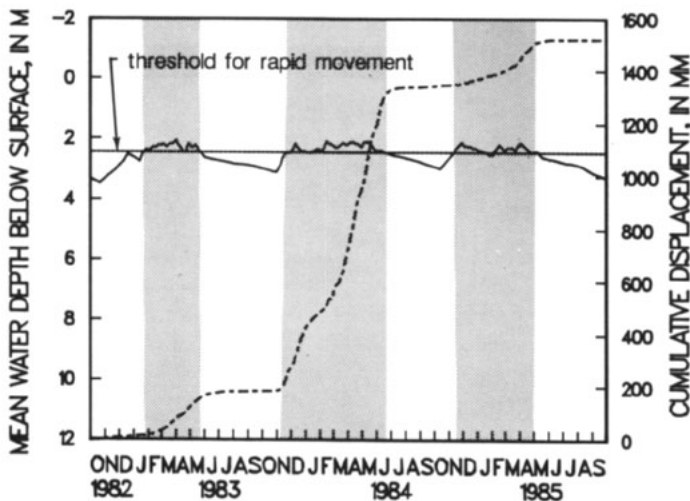


Figure 14. Cumulative landslide displacement measured at the extensometer site (dashed line) and the mean water level in intermediate-depth wells (compare with Figs. 4 and 10). Periods of relatively rapid displacement (shaded regions) correspond closely with periods when the mean water level in intermediate-depth wells exceeds a threshold.

its thickness (Figs. 1 and 3), and so the assumption of infinite areal extent is quite good. The classic infinite-slope equation (for example, see Taylor, 1948, p. 431) also assumes, however, that ground water flows parallel to the ground surface, an assumption not satisfied at Minor Creek landslide. Here we use a simple extension of the limit-equilibrium theory of Iverson and Major (1986) to generalize the classic infinite-slope equation so that it accounts for flow that is not parallel to the surface. For incipient motion, this yields the normalized force balance (R. M. Iverson, unpub. derivation):

$$\frac{-\sin(\beta - \phi) + (c \cos \phi)/gA}{\sin(\lambda + \phi)} = Z \quad (4a)$$

where

$$A = (\rho_t - \rho_w)(T-d) + \rho_u d \quad (4b)$$

and

$$Z = i \rho_w (T-d)/A \quad (4c)$$

in which  $\phi$  is the residual friction angle of the soil;  $c$  is its residual cohesion;  $\rho_t$  is its saturated, total mass density;  $\rho_u$  is its mean unsaturated mass density above the water table;  $\rho_w$  is the mass density of water;  $d$  is the water-table depth;  $i$  is the magnitude of the hydraulic head gradient;  $T$  is the landslide thickness;  $\beta$  is the slope angle;  $g$  is the magnitude of gravitational accel-

eration; and  $\lambda$  is the angular direction of groundwater seepage (Fig. 11). For the case of zero residual cohesion, which we assume for Minor Creek landslide, equation 4a reduces to the equation derived by Iverson and Major (1986), with  $Z$  modified slightly to account for a non-zero water-table depth. The general solution of Iverson and Major (1986), plotted here as Figure 15, can therefore be used to understand how hydraulic gradients and ground-water flow control the balance of forces that instigate seasonal landslide motion.

We illustrate the way in which hydraulic gradients and other physical parameters affect the balance of forces at Minor Creek landslide by substituting representative parameter values into equations 4, solving for the residual friction angle, and assessing the sensitivity of the solution. From Table 1, Figure 10, Figure 11, and inclinometer data (Iverson, 1984), we obtain representative parameter values that apply during incipient motion:  $\rho_t = 2,230 \text{ kg/m}^3$ ;  $\rho_u = 2,100 \text{ kg/m}^3$ ;  $\rho_w = 1,000 \text{ kg/m}^3$ ;  $d = 0.4 \text{ m}$ ;  $i = 0.63$ ;  $T = 6 \text{ m}$ ;  $\beta = 15^\circ$ ; and  $\lambda = 157^\circ$ . Substituting these values into equations 4, we find that limiting equilibrium is satisfied if  $\phi = 17.5^\circ$ . This result for  $\phi$  is modified by less than half a degree if we assume that a residual cohesion of up to  $1,000 \text{ N/m}^2$  contributes to the soil strength. Similarly, the result is quite insensitive to the water-table depth, changing  $\phi$  by less than half a degree if we change the depth by less than 1 m.

In sharp contrast, the result is very sensitive to the hydraulic gradient. Figure 15 shows this graphically: with  $\phi = 17.5^\circ$ , our limit-equilibrium values  $\lambda + \phi = 174.5^\circ$ ;  $\beta - \phi = -2.5^\circ$ ; and  $Z = 0.46$  determine a failure point on Figure 15 that falls in the vicinity of very closely spaced curves. Thus the value of  $\phi$  required for limiting equilibrium can shift significantly if changes in the direction or magnitude of the hydraulic gradient occur.

Further limit-equilibrium calculations help to quantify the delicate balance between frictional resisting forces and the destabilizing influence of the prevailing ground-water flow field at Minor Creek landslide. During the wet season, both the magnitude of the mean hydraulic gradient and the height of the water table are somewhat greater than in the dry season (Fig. 10). These two factors combine to instigate seasonal motion, but their effect on the landslide's stress state is small compared to effects that would result from significant flow-field modification. We know empirically, for example, that a dry-season water-table decline of 1 m and mean hydraulic gradient reduction to half its wet-season magnitude reduces stresses sufficiently from limit-equilibrium levels that landslide motion is stopped (compare Figs. 10 and 14). But equation 4a and Figure 15 show that the landslide would continue moving under these dry-season stresses if its residual friction angle were reduced by only about one degree. In contrast, if ground water flowed parallel to the ground surface ( $\lambda = 90^\circ$ ), driven by a gradient  $i = \sin \beta = 0.26$ ,  $\phi$  would have to increase from  $17.5^\circ$  to  $25^\circ$  to maintain wet-season equilibrium. If the same slope-parallel flow were driven by our measured wet-season gradient,  $i = 0.63$ , maintenance of equilibrium would require that  $\phi = 36^\circ$ ! Clearly, both the direction and magnitude of the hydraulic gradient strongly influence limit-equilibrium conditions for landslide motion, and the adjustment between the prevailing gradient and seasonal motion at Minor Creek landslide is finely tuned.

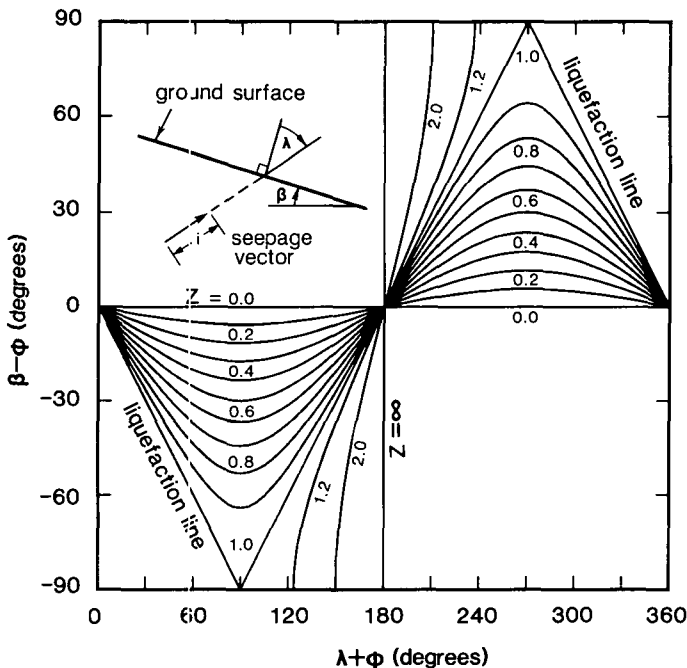


Figure 15. Plot of the solution of equation 4a with  $c = 0$ , showing the normalized relationship between the limiting slope angle ( $\beta$ ), seepage direction ( $\lambda$ ), and friction angle ( $\phi$ ) in cohesionless, infinite slopes for different values of  $Z$ . Liquefaction pre-empts Coulomb failure in the zones outside the liquefaction lines (after Iverson and Major, 1986).

On the basis of our detailed head measurements, we are confident that the mean hydraulic gradient that triggers seasonal motion at Minor Creek landslide corresponds well with the typical wet-season gradient shown in Figure 11. Nonetheless, the wet-season flow field may vary from place to place (Fig. 12), and the spatial variations may cause localized stresses that perturb the typical pattern of seasonal motion.

#### Spatially Variable Flow and Perturbations of Motion

Spatial variations in the ground-water flow field produce seepage forces that also are spatially variable. The seepage force field coincides with the negative of the hydraulic gradient field in a saturated, isotropic soil, and it represents the only force other than buoyancy and weight that ground water exerts on the soil (compare Lambe and Whitman, 1979, p. 261–263). Figure 15 shows that slope instability is universally maximized by seepage forces that are directed so that  $\lambda = 90^\circ - \phi$ . At Minor Creek landslide, where  $\phi$  is nearly equal to the slope angle, the seepage direction that maximizes instability is therefore almost horizontal. Consequently, it is important to identify places where ground water may flow almost horizontally and perhaps emerge at the ground surface.

Our model results (Fig. 12) and qualitative field observations both indicate that emergent seepage can occur locally at the bases of steep hummock faces on Minor Creek landslide. We also infer that the elastic stress field near the bases of hummock faces favors instability because high shear stresses and low normal stresses commonly are focused near such points (Savage and others, 1985). Although our measurements of emergent seepage are scarce, it is not surprising that when rapid motion and deformation of Minor Creek landslide occur, we observe ground breakage and surficial failures that commonly begin near the bases of steep sections of the landslide. Theoretical results show that localized zones of perturbed motion that begin in this way may, with time, spread from their source and influence a large part of the landslide (Iverson, 1986a, 1986c). Indeed, seasonal movement that was perturbed by erosion of the toe of Minor Creek landslide (Iverson, 1984) may be responsible for the steepness of the cumulative movement curve for water year 1984 (Fig. 14).

The inherent instability caused by ground-water flow and stress fields influenced by hummocky microtopography tempts us to conjecture

about the long-term behavior of unstable ground: hummocky microtopography enhances local instability, which in turn may lead to local failures that create new hummocks. That is, a positive feedback mechanism might exist, whereby unstable, hummocky ground becomes more unstable until the mean slope is flattened appreciably or a cataclysmic failure occurs. Such fundamentally unstable behavior might explain the widely divergent movement rates observed on morphologically similar landslides in northwestern California (compare Kelsey, 1978).

#### CONCLUSIONS

Field data and inferences from physically based theory support the following conclusions about the relationships between ground-water flow and seasonal landslide movement.

1. The basal shear zone of Minor Creek landslide is virtually always saturated, and nearly the entire landslide is saturated during the winter wet season, when landslide movement occurs. Complete saturation means that topographic elevation provides the dominant force potential that drives ground-water flow.

2. The ground-water flow field in Minor Creek landslide varies considerably in time and space, but the mean hydraulic gradient is directed mostly downward. Many data need to be averaged to construct a simple, quantitative flow net that depicts the mean gradient. Indeed, even with the high spatial density of the data we use, we cannot construct a more detailed, empirical flow net without making many subjective interpretations. We consequently are skeptical of analyses that employ few data and make "standard" assumptions (such as that of slope-parallel flow) about how ground water affects slope stability.

3. Representative values of the hydraulic conductivity and diffusivity of the soil in Minor Creek landslide are  $5 \times 10^{-8}$  m/s and  $1 \times 10^{-6}$  m<sup>2</sup>/s. These values are within the range anticipated for the landslide's poorly sorted, clay-rich soil. Owing to soil heterogeneity, however, the values can vary over several orders of magnitude.

4. With increasing depth, transient ground-water responses to rainfall increasingly attenuate and lag behind the rainfall. Transient ground-water responses early in the wet season can be influenced strongly by antecedent water storage in the unsaturated zone, whereas responses later in the wet season are directly related to pore-pressure transmission that accompanies saturated ground-water flow. A simple linear model

for diffusive propagation of pore-pressure waves provides an accurate theoretical framework for interpreting the wet-season ground-water responses. The model shows how diffusion attenuates high-frequency head responses, such as might result from individual rainstorms, so that they become indistinguishable before they reach the landslide base. In contrast, low-frequency head responses, such as might result from monthly or yearly rainfall cycles, are clearly evident at the landslide base. Such behavior is not unique to Minor Creek landslide; similar attenuation of pore-pressure waves has been observed in other slopes where the hydraulic diffusivity is low (Kenney and Lau, 1984).

5. Times of high ground-water head at the base of Minor Creek landslide coincide with times when there is a relatively steady, wet-season head distribution that instigates seasonal landslide motion. The stress state at incipient motion is very sensitive to the ground-water head distribution. The delicate balance that exists between seasonal changes of the ground-water flow field and seasonal landslide movement shows that if the slope angle, thickness, strength, or hydrology of the landslide were changed even moderately, significant departures from the current landslide behavior could result. In the sense described by Gilbert (1877), we would say that the geometry and motion of the landslide are graded to the material properties and hydrology of the slope.

6. We infer from theory and qualitative observations that local ground-water circulation can perturb the over-all stress state and pattern of motion at Minor Creek landslide. Local circulation may result either from subsurface flow barriers or from head gradients caused by hummocky microtopography. Hummocks can cause local recharge on relatively flat sections of the slope and discharge near the bases of steep sections of the slope. Outward-directed seepage in the discharge areas makes them likely candidates for local instability and perturbed movement that can spread to adjacent parts of the landslide.

#### ACKNOWLEDGMENTS

The senior author thanks John Bredehoeft, Dick Janda, and Mike Nolan for helping to motivate this study and Bern Hinckley and Barry Hill for their help with installing and maintaining the field instrumentation. We thank Rex Baum, Brann Johnson, Harvey Kelsey, Tom Winter, and Bob Ziemer for their helpful reviews of the manuscript. Paul Holm and the

Barnum Timber Company cordially permitted us to work on their land. This project began as part of the senior author's dissertation work at Stanford University, where Irwin Remson, Joe Franzini, David Freyberg, and Ed Kavazanjian provided advice and moral support.

## REFERENCES CITED

- Bear, J., 1979, *Hydraulics of groundwater*: New York, McGraw-Hill, 567 p.
- Bertini, T., Cugusi, F., D'Elia, B., and Rossi-Doria, M., 1984, Climatic conditions and slow movements of colluvial covers in central Italy: 4th International Symposium on Landslides, Proceedings, Toronto, p. 367-376.
- Bouwer, H., and Rice, R. C., 1976, A slug test for determining hydraulic conductivity of unconfined aquifers with completely or partially penetrating wells: *Water Resources Research*, v. 12, p. 423-428.
- Bromirski, P., and Dengler, L., 1985, Seismic refraction study of an earthflow in Redwood Creek basin, northwestern California [abs.]: EOS (American Geophysical Union Transactions), v. 66, no. 46, p. 889.
- Carlsaw, H. S., and Jaeger, J. C., 1959, *Conduction of heat in solids*: Oxford, England, Oxford University Press, 510 p.
- Colman, S. M., 1973, The history of mass movement processes in the Redwood Creek basin, Humboldt County, California [M.S. Paper]: University Park, Pennsylvania, The Pennsylvania State University, 180 p.
- Cooley, R. L., 1983, Some new procedures for numerical solution of variably saturated flow problems: *Water Resources Research*, v. 19, p. 1271-1285.
- Eagleson, P. S., 1970, *Dynamic hydrology*: New York, McGraw-Hill, 462 p.
- Freeze, R. A., and Witherspoon, P. A., 1966, Theoretical analysis of regional groundwater flow. 1. Analytical and numerical solutions to the mathematical model: *Water Resources Research*, v. 2, p. 641-656.
- , 1967, Theoretical analysis of regional groundwater flow. 2. Effect of water-table configuration and subsurface permeability variation: *Water Resources Research*, v. 3, p. 623-634.
- Freeze, R. A., and Cherry, J. A., 1979, *Groundwater*: Englewood Cliffs, New Jersey, Prentice-Hall, 664 p.
- Gambolati, G., 1973, Equation for one-dimensional vertical flow of groundwater. 2. Validity range of the diffusion equation: *Water Resources Research*, v. 9, p. 1385-1395.
- Gilbert, G. K., 1877, *Geology of the Henry Mountains (Utah)*: U.S. Geological and Geographical Survey of the Rocky Mountain Region: Washington, D.C., U.S. Government Printing Office.
- Gillham, R. W., 1984, The capillary fringe and its effect upon water-table response: *Journal of Hydrology*, v. 67, p. 307-324.
- Harden, D. R., Janda, R. J., and Nolan, K. M., 1978, Mass movement and storms in the drainage basin of Redwood Creek, Humboldt County, California—A progress report: U.S. Geological Survey Open-File Report 78-486, 161 p.
- Harden, D. R., Kelsey, H. M., Morrison, S. D., and Stephens, T. A., 1982, *Geologic map of the Redwood Creek drainage basin, Humboldt County, California*: U.S. Geological Survey Water-Resources Investigations Open-File Report 81-496, 1 sheet.
- Hodge, R. A. L., and Freeze, R. A., 1977, Groundwater flow systems and slope stability: *Canadian Geotechnical Journal*, v. 14, p. 466-476.
- Humphreys, N. F., 1982, Pore pressures in debris failure initiation: Project report, project no. A-108-WASH: State of Washington Water Research Center, Washington State University and The University of Washington, 169 p.
- Iverson, R. M., 1984, Unsteady, nonuniform landslide motion: Theory and measurement [Ph.D. dissert.]: Stanford, California, Stanford University, 303 p.
- , 1985a, Minor Creek landslide, in Savina, M. E., ed., *Redwood country: American Geomorphological Field Group, 1985 Conference, Field Trip Guidebook*, p. 40-50.
- , 1985b, A constitutive equation for mass-movement behavior: *Journal of Geology*, v. 93, p. 143-160.
- , 1986a, Dynamics of slow landslides: A theory for time-dependent behavior, in Abrahams, A. D., ed., *Hillslope processes*: Winchester, Massachusetts, Allen & Unwin, p. 297-317.
- , 1986b, Unsteady, nonuniform landslide motion: 1. Theoretical dynamics and the steady datum state: *Journal of Geology*, v. 94, p. 1-15.
- , 1986c, Unsteady, nonuniform landslide motion: 2. Linearized theory and the kinematics of transient response: *Journal of Geology*, v. 94, p. 349-364.
- Iverson, R. M., and Major, J. J., 1986, Groundwater seepage vectors and the potential for hillslope failure and debris flow mobilization: *Water Resources Research*, v. 22, p. 1543-1548.
- Janda, R. J., 1979, Summary of regional geology in relation to geomorphic form and process, in *Guidebook for field trip to observe natural and management-related erosion in Franciscan terrane of northern California*: Geological Society of America Annual Meeting, Cordilleran Section, San Jose, California, p. 11-11-15.
- Keefer, D. K., and Johnson, A. M., 1983, Earthflows: Morphology, mobilization, and movement: U.S. Geological Survey Professional Paper 1264, 56 p.
- Kelsey, H. M., 1978, Earthflows in Franciscan melange, Van Duzen River basin, California: *Geology*, v. 6, p. 361-364.
- Kenney, C., 1984, Properties and behavior of soils relevant to slope instability, in Brunson, D., and Prior, D. B., eds., *Slope instability*: New York, Wiley, p. 27-65.
- Kenney, T. C., and Lau, K. C., 1984, Temporal changes in groundwater pressure in a natural slope of nonfissured clay: *Canadian Geotechnical Journal*, v. 20, p. 138-146.
- Lambe, T. W., and Whitman, R. V., 1979, *Soil mechanics*, SI version: New York, Wiley 553 p.
- Leach, B., and Herbert, R., 1982, The genesis of a numerical model for the study of the hydrogeology of a steep hillside in Hong Kong: *Engineering Geology Quarterly Journal*, v. 15, p. 243-259.
- Mitchell, J. K., 1976, *Fundamentals of soil behavior*: New York, Wiley, 422 p.
- Nadler, D. E., 1984, *Groundwater hydrology and slope movement at Pavilion, B.C.* [M.S. thesis]: Vancouver, British Columbia, University of British Columbia, 138 p.
- Narasimhan, T. N., 1982, Physics of unsaturated-saturated subsurface flow, in Narasimhan, T. N., ed., *Recent trends in hydrogeology*: Geological Society of America Special Paper 189, p. 3-24.
- Nolan, K. M., Harden, D. R., and Colman, S. M., 1976, Erosional landform map of the Redwood Creek drainage basin, Humboldt County, CA, 1947-74: U.S. Geological Survey Open-File Report 76-42, 1 sheet.
- Nolan, K. M., and Janda, R. J., in press, Sediment discharge and movement of two earthflows in Franciscan terrane, northwestern California, in Nolan, K. M., Marron, D. C., and Kelsey, H. M., eds., *Geomorphic processes and aquatic habitat in the Redwood Creek basin, northwestern California*: U.S. Geological Survey Professional Paper 1454.
- Patton, F. D., and Hendron, A. J., 1974, General report on mass movements: 2nd International Congress of the International Association of Engineering Geologists, Sao Paulo, Brazil, Proceedings, v. 2, p. V-GR-1-V-GR-57.
- Prior, D. B., and Stephens, N., 1972, Some movement patterns of temperate mudflows: Examples from northeastern Ireland: *Geological Society of America Bulletin*, v. 83, p. 2533-2544.
- Reid, M. E., Nielsen, H. P., and Dreiss, S. J., 1985, Pore pressure response during recent slope failure: *Geological Society of America Abstracts with Programs*, v. 17, no. 7, p. 698.
- Sangrey, D. A., Harrop-Williams, K. O., and Klaiber, J. A., 1984, Predicting ground-water response to precipitation: *American Society of Civil Engineers Journal of Geotechnical Engineering*, v. 110, p. 957-975.
- Savage, W. Z., Swolfs, H. S., and Powers, P. S., 1985, Gravitational stresses in long symmetric ridges and valleys: *International Journal of Rock Mechanics, Mining Sciences, and Geomechanics Abstracts*, v. 22, p. 291-302.
- Swanson, F. J., Graham, R. L., Lienkaemper, G. W., and Harr, R. D., 1983, Movement of Lookout Creek earthflow, western Cascades, Oregon, 1974-1982 [abs.]: Association of Engineering Geologists Annual Meeting, Abstracts with Programs, p. 95.
- Swanston, D. N., Ziemer, R. R., and Janda, R. J., 1983, Influence of climate on progressive hillslope failure in Redwood Creek valley, northwestern California: U.S. Geological Survey Open-File Report 83-259, 42 p.
- Taylor, D. W., 1948, *Fundamentals of soil mechanics*: London, England, Wiley, 700 p.
- Terzaghi, K., 1923, Die Berechnung der Durchlässigkeitsziffer des Tonens aus dem Verlauf der hydrodynamischen Spannungserscheinungen, *Sitzungsberichte der Akademie der Wissenschaften in Wien: Mathematisch-naturwissenschaftliche Klasse*, Part 2a, v. 132, no. 3/4.
- , 1943, *Theoretical soil mechanics*: New York, Wiley, 510 p.
- , 1950, Mechanism of landslides, in Paige, S., ed., *Application of geology to engineering practice* (Berkey Volume): New York, Geological Society of America, p. 83-123.
- Toth, J., 1963, A theoretical analysis of groundwater flow in small drainage basins: *Journal of Geophysical Research*, v. 68, p. 4795-4812.
- Vandine, D. F., 1980, *Engineering geology and geotechnical study of Drynoch landslide, British Columbia*: Geological Society of Canada Special Paper 79-31.
- Varnes, D. J., 1978, Slope movement types and processes, in Schuster, R. L., and Krizek, R. J., eds., *Landslides analysis and control*: Washington, D.C., Transportation Research Board Special Report 176, National Academy of Sciences, p. 11-33.
- Wasson, R. J., and Hall, G., 1982, A long record of mudslide movement at Waerenga-O-Kuri, New Zealand: *Zeitschrift für Geomorphologie, Supplementband*, v. 26, p. 73-85.
- Wilson, C. J., Reneau, S. L., Dietrich, W. E., and Narasimhan, T. N., 1984, Modeling the generation of excessive pore pressures in debris flow susceptible deposits [abs.]: EOS (American Geophysical Union Transactions), v. 65, p. 889.
- Winter, T. C., 1983, The interaction of lakes with variably saturated porous media: *Water Resources Research*, v. 19, p. 1203-1218.
- Wolff, R. G., and Olsen, H. W., 1968, Piezometer for monitoring rapidly changing pore pressures in saturated clays: *Water Resources Research*, v. 14, p. 839-843.
- Ziemer, R. R., 1984, The response of progressive hillslope deformation to precipitation, in O'Loughlin, C. L., and Pearce, A. J., eds., *Symposium on Effects of Forest Land Use on Erosion and Slope Stability*, 7-11 May 1984, Honolulu, Hawaii, Proceedings: International Union Forest Research Organizations, p. 91-98.

MANUSCRIPT RECEIVED BY THE SOCIETY JUNE 23, 1986  
 REVISED MANUSCRIPT RECEIVED MARCH 2, 1987  
 MANUSCRIPT ACCEPTED MARCH 25, 1987